Control of Antagonistic McKibben Muscles via a Bio-inspired Approach

Xinyi Chen[1], Wenxin Zhu[1], Wenyu Liang[2], Yilin Lang[1], Qinyuan Ren[1*]

[1]State Key Laboratory of Industrial Control Technology, Zhejiang University, Hangzhou, Zhejiang, Hangzhou, China, 310027.
[2]Institute for Infocomm Research, A*STAR, Singapore, 138632.

*Corresponding author(s). E-mail(s): renqinyuan@zju.edu.cn;

Abstract

McKibben muscles are increasingly used in many robotic applications due to their advantages of lightweight, compliant, and skeletal muscles-like behaviours. However, there are still huge challenges in the motion control of McKibben muscles due to the system nonlinearity (e.g., hysteresis) and model uncertainties. To investigate the control issues, a soft artificial arm actuated by an antagonistic pair of McKibben muscles, mimicking the biological structure of skeleton-muscle systems, is developed. Inspired by the biological motor control capability that humans can control and coordinate a group of muscles to achieve complex motions, a cerebellum-like controller based on Spiking Neural Networks (SNNs) is employed for the motion control of the developed artificial arm. Benefit from the employment of the SNN-based cerebellar model, the proposed control scheme provides online adaptive learning capability, good computational efficiency, fast response, and strong robustness. Finally, several simulations and experiments are conducted subject to different environmental disturbances. Both simulation and experimental results verify that the proposed method can achieve good tracking performance, adaptability, and strong robustness.

Keywords: McKibben muscle; Cerebellum-like controller; Spiking neural network; Soft artificial arm; Adaptive control.

1 Introduction

McKibben muscles, which are lightweight, compliant, and able to generate analogous behaviours like skeletal muscles, are attracting increasingly great attention in robotics. Owing to their compliance and high power density, McKibben muscles can be potentially employed as bionic actuators for many bio-inspired robotic applications, such as robot manipulators [1, 2], exoskeletons [3, 4], medical robots [5], human-robot interaction [6], etc. However, in these studies, the motion control of McKibben-actuated systems has been proven challenging due to the highly nonlinear behaviours and model uncertainties of the soft actuators.

Previous studies on the control of McKibben muscles can be mainly divided into two categories: model-based control and data-driven-based control. The former category first establishes analytical models to represent the behaviours of McKibben muscles and then designs control strategies based on the established models to regulate the McKibben muscle-actuated systems. To compensate for the nonlinear behaviour of the McKibben muscle motions, model-based feed-forward controllers are commonly used and the notable examples include the studies presented in [7, 8]. However, in these studies, due to the lack of feedback information, the systems are susceptible to environmental disturbances. To enhance the system robustness, feedback control schemes are employed in several studies. In [9], a systematic study on position control of McKibben muscles using classic Proportional-Integral-Derivative (PID) controller was conducted. In [10], a model-based Sliding Mode Control (SMC) approach was introduced for controlling the pneumatic muscle actuators in different configurations. To better handle the dynamic model uncertainties, the research presented in [11] investigated adaptive control strategies of pneumatic muscle actuators for an artificial elbow. Indeed, feedback control is an effective way to deal with system parameter uncertainties, but the model accuracy could also impact the control performance significantly. It is worth noting that the dynamics of a McKibben muscle-actuated system and the joint stiffness are always time-varying, which leads to huge challenges in obtaining an accurate analytical model of McKibben muscles.

An alternative control approach for McKibben muscles is the data-driven-based control, which is to infer dynamics relationships from the input-output data. In [12], a neural map algorithm was employed to control a pneumatic robotic arm through the feedback information from two cameras. In [13], a model-free adaptive iterative learning algorithm was presented to control a McKibben muscle suspended on a rigid frame. In [14], an Adaptive Recurrent Neural Network (ARNN) was designed to control a pneumatic muscle-driven manipulator for real-time human-friendly industrial applications. These control systems show good performances in the their particular tasks, but the pure data-driven approaches are usually lack of generalization in different environments.

Due to the similar properties between McKibben muscles and skeletal muscles, such as nonlinearity, compliance, and viscoelasticity, several studies exploited the control mechanism of skeletal muscles and further apply the bio-inspired control mechanism to control McKibben muscles. Biologically, it has been confirmed that the cerebellum is the coordination center of human beings and crucial for skeletal muscle control. The computational capacity of the cerebellum as a learning device

was evaluated through anatomy and physiology evidences in [15, 16]. As pointed in [17], from a perspective of cybernetics, the cerebellar function can be considered as a set of adaptive filters or internal models to coordinate the motor behaviours of muscles. Inspired by this discovery, a cerebellar-inspired adaptive controller is proposed in [18] to control a robot eye actuated by McKibben muscles. In this study, the controller imitates the function of the cerebellum to compensate for the uncertainties of the rough inverse plant model. Particularly, the control performance of the robot eye validated the fact through experiments that the model of cerebellar function may help the system overcome the challenges of controlling McKibben muscles in real-world applications.

Similar to skeletal muscles, McKibben muscles are usually operated in antagonistic pairs in many applications, especially for rehabilitation robots [19, 20] and humanoid robots [21, 22]. The main reason of adopting the antagonistic configuration is that it enables the McKibben muscle-driven system to generate symmetrical bidirectional motion as well as to achieve high and adjustable joint stiffness [4, 23]. Nevertheless, as pointed from [24], due to the nonlinearity of McKibben muscles and the redundant setup, the motion of antagonistic Mckibben muscles is difficult to be precisely modelled in an analytical form. Thus, in [25], a Reinforcement Learning (RL)-based approach, a kind of data-driven approach, was proposed to estimate the inverse model of a set of antagonistic McKibben muscles for the control purpose. However, in these studies, the enhancement of the system robustness and the expedition of the RL processing are still under research. This paper aims to investigate the control issues of the antagonistic McKibben muscles from a bio-inspired respective. To facilitate this investigation, an artificial arm actuated by a pair of antagonistic McKibben muscles is developed. For the controller design purpose, the behaviours of the arm is first modelled and analyzed. Following that, inspired by the motor control loop in the biological nervous system, a cerebellum-like control scheme based on the model analysis for the motion control of the developed arm is proposed.

Remarkably, benefit from the unique neural coding scheme in the neural circuit called "spikes", the nervous system shows an attractive cognitive capacity where it could integrate various sensorimotor information over time and derive rapid and accurate responses. Hence, Spiking Neural Networks (SNNs), which was first introduced in [26] in 1952, are adopted to implement spatio-temporal dynamics to mimic the sparse information representation and the asynchronous computation mechanism in the nervous system. In the proposed control scheme, different from the traditional Cerebellar Model Articulation Controller (CMAC) first introduced in [27] in 1975, a cerebellar model based on spiking dynamics that is similar to the neurobiological properties of the biological neurons is established. Here, an online learning mechanism is designed in this model so that the antagonistic pair of McKibben muscles can be controlled adaptively through compensating for the model uncertainties. Moreover, due to the synaptic plasticity in the employed cerebellar model, namely, Spike-Timing-Dependent Plasticity (STDP) mechanism with eligibility trace, the proposed controller can handle the online error-correction with hundreds of milliseconds of delay. Furthermore, SNNs are more competitive than the state-of-the-art Artificial Neural Networks (ANNs) in handling the control problems of

antagonistic McKibben muscles, which mainly comes down to these reasons: (i) The synaptic weights in SNNs are updated by local learning rules (e.g., STDP) without requiring the backpropagation of global errors commonly used in ANNs, which can improve the computational efficiency [28]. (ii) In SNNs, the output neural layer could response immediately on the incoming spikes from sensors, whereas ANNs have to wait for multiple time-steps. In this way, SNNs could record dynamic changes in real-time and fully exploit the temporal information, which is crucial for controlling systems with high latency [29]. (iii) The SNN-based controllers exhibit strong noise robustness while other control schemes are always susceptible to noise and temporal jitter that are commonly presented in sensory information [30]. To our best knowledge, this paper is the first study on control McKibben muscle-actuated systems based on a cerebellum-like SNN model.

The rest of this paper is organized as follows. The model of the antagonistic McKibben muscles is detailed in Section 2. Section 3 proposes the cerebellar control method. The simulation and experimental results are presented in Section 4. Finally, Section 5 gives the conclusions.

2 Antagonistic McKibben Muscles

In this section, the mechanical design of the antagonistic McKibben muscles is first presented and then follow by a presentation of the system modelling.

2.1 Mechanical Design

In human limbs, groups of skeletal muscles usually attach to skeletons in antagonistic pairs. As shown in Figure 1(a), the rotation motion of the elbow joint is actuated by a coactivation of the biceps and triceps, namely, the flexor muscle and the extensor muscle, respectively. Through the coordination of these groups of muscles, humans could generate versatile Degree-of-Freedom (DoF) behaviours. Inspired by such biological system, a pneumatic artificial arm is developed to investigate the control issues of the antagonistic McKibben muscles, corresponding to the mechanical system shown in Figure 1(b). As can be seen, the two ends of each McKibben muscle are mounted to a 1:1 model of skeleton frame by the iron hoops. Each McKibben muscle of the artificial arm is made up of an inner tube with inflatable latex and a surrounding braided sleeve, which is driven by the input airflow generated from an air pump. The amount of the input airflow is regulated by an electromagnetic valve and a pressure sensor is equipped on the intake pipe to measure the pressure inside the McKibben muscle.

The antagonistic pair of the McKibben muscles could actuate the motions of the elbow joint collaboratively. For example, when the arm is lifted up, one muscle will stretch and the another one will contract, similar to the function of the extensor muscle and the flexor muscle.

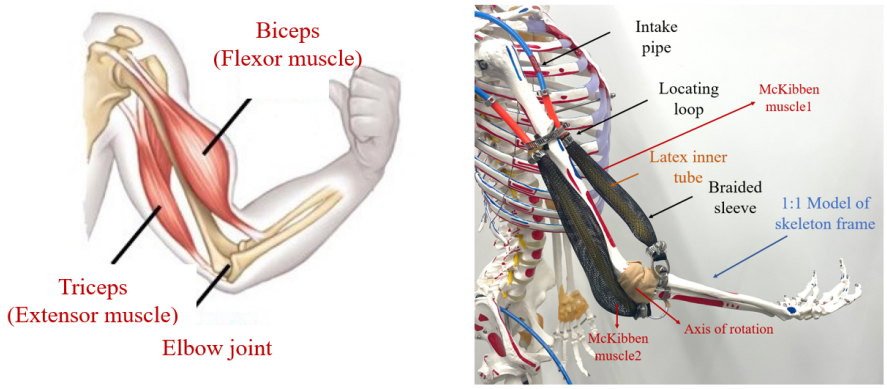

(a) (b)

Fig. 1 The biomimetic design of the artificial arm: (a) Biological antagonistic muscles attached on human bones; (b) The mechanical configuration of the developed artificial arm.

2.2 Modelling

Figure 2 illustrates the modelling schematic diagram of the artificial arm. The process of establishing the coordinate system is as follows: Initially, set the angular motion of the planar articulated artificial arm in the x-y plane, and set the elbow joint as the original point O, then set the central axis of the upper arm as the x-axis, and finally establish the y-axis through the right-hand rule. Furthermore, the angular position of the forearm is represented as θ. Figure 2 (a) shows the state when $\theta = 0$, which is defined as the initial state, and Figure 2 (b) illustrates the state when forearm lifts at the angle of θ. The lengths of the flexor and extensor muscles are defined as l_1, l_2, respectively.

As pointed in [32], the kinematic model of the muscle system can be described as

$$l_1(t) = \sqrt{D_1^2 + D_2^2 - 2D_1D_2\cos(\pi - \theta(t))}, \tag{1}$$

$$l_2(t) = D_3 + D_4 + 2D_0 \sin\left(\frac{\theta(t)}{2}\right). \tag{2}$$

In the above kinematic model, the lengths of the McKibben muscles $l_1(t), l_2(t)$ are calculated geometrically as a function of the lift angle $\theta(t)$. The kinematics only takes into account the changes in muscle lengths, i.e., axial stretch/constriction. Actually, the physical change of each McKibben muscle during actuation includes both axial and radial deformations. This radial deformation, which is usually hard to be measured, can be treated as a kind of uncertainties of the system and then compensated by a robust control scheme.

For a single McKibben muscle, the contraction of the length is generated by the contraction force of the inner tube imposed with internal pressures. In this work, the well-known Chou-Hannaford model presented in [33] is adopted for modelling the dynamics of the McKibben muscle. It is worth to be noted that this model is

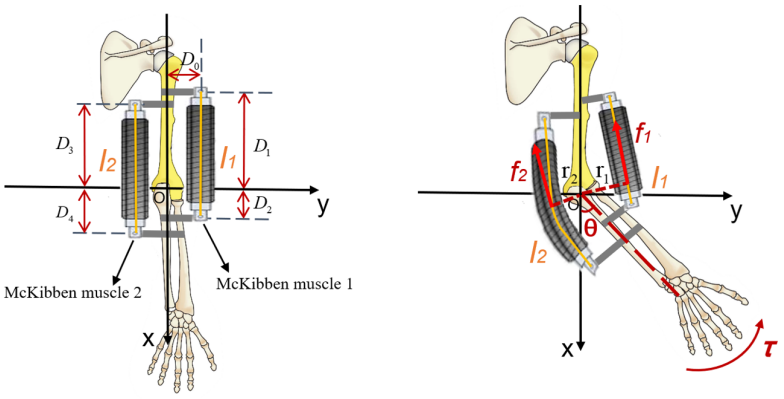

(a) Initial (b) Lift

Fig. 2 The modelling schematic diagram of the artificial arm. Inspired by the anatomical characteristics of elbow joints [31], the skeleton frame of the developed artificial arm can be regarded as a rigid body in terms of material properties. The upper arm remains fixed while radius and the lower arm performs flexion and extension to restrict the elbow joint motion in a sagittal plane. Both McKibben muscles stay completely symmetric to the sagittal plane due to the mechanical constraint. (a) Initial ($\theta = 0$): each endpoint of the McKibben muscles is D_0 away from the x-axis, and the distances from the endpoints of the McKibben muscles to the y-axis are defined as D_1, D_2, D_3, D_4, respectively. (b) Lift ($\theta \neq 0$): the arm generates torques via the forces of the antagonistic McKibben muscles.

valid based on a set of assumptions discussed in [34], such as the inner tube is thin-walled, the McKibben muscle keeps a cylindrical shape throughout the contraction, the friction can be ignored during contraction, and etc. Restricted to these assumptions, the actual model of the McKibben muscle with the addition of uncertainties can be expressed as

$$f_i = k_i(l_i^2 - \bar{l}_i^2)p_i + \chi(l_i, q_m, V), \tag{3}$$

where f_i denotes the force provided by the i-th McKibben muscle, p_i denotes the pressure in the inner tube of the i-th McKibben muscle, l_i is corresponding to the length of the i-th McKibben muscle, $\bar{l}_i$ is the initial length that measured at rest with zero gage pressure, k_i is a constant parameter, q_m is the mass flow of input air flow, V is the chamber working volume of the McKibben muscle, $\chi(l_i, q_m, V)$ can be considered as the model uncertainties in the dynamic model of the McKibben muscle.

For the entire skeleton-muscle system consisting of an antagonistic pair of McKibben muscles, the rotational motion is driven by the forces exerted by the antagonistic McKibben muscles. Hence, the dynamic model of the antagonistic muscle pairs can be described as

$$I\ddot{\theta} = f_1 r_1 - f_2 r_2 + \chi(\theta, \dot{\theta}, q_m, V), \tag{4}$$

where r_1 and r_2 are one-to-one corresponding to the moment arms of McKibben muscle 1 and McKibben muscle 2, I denotes the moment of inertia of the revolute joint, $\chi(\theta, \dot{\theta}, q_m, V)$ contains the system dynamics (i.e., stiffness, damping), aerodynamics of muscles caused by air flow, and the torque caused by gravity and external disturbances.

In summary, the force generated by the antagonistic pair of McKibben muscles can be divided into three parts. One is the force generated by the axial length change, which is represented by the dynamic model as shown in Equation (3). However, with the contraction of the muscle, the braided sleeve bends at both ends, resulting in the deviation of the model. The other part is the axial force generated by the radial deformation of the soft material. The final part subjects to the rate of input airflow and the effects of thermodynamic processes in the flow. In fact, it is difficult to model all parts of the force accurately. Thus, for control purpose, $\chi(\theta, \dot{\theta}, q_m, V)$ can be treated as model uncertainties and then compensated by the control scheme proposed in the next Section. In addition, the control objective in this study is to investigate the precision motion control of the pair of antagonistic McKibben muscles, hence, the controller is required to adaptively handle the kinematic/dynamic uncertainties of both McKibben muscles, simultaneously.

3 Cerebellum-like Control Scheme

In this section, a bio-inspired cerebellum-like SNN is proposed and elaborated to control the antagonistic McKibben muscle pairs without accurate prior models.

3.1 Cerebellar Control Loop

In biological system, the cerebellum plays a significant role in fine motor control, coordination of motor processes as well as learning of motor tasks. Figure 3 illustrates a simplified schematic representation of the cerebellar structure. The cerebellum is composed of three types of fibers: Mossy Fiber (MF), Parallel Fiber (PF) and Climbing Fiber (CF), as well as seven kinds of cells: Granule Cell (GR), Purkinje Cell (PC), Deep Cerebellar Nuclei (DCN), Inferior Olive Nucleus Cell (IO), Golgi Cell (GgC), Basket Cell (BC) and Stellate Cell (SC) [35].

Cooperating with the cerebellum, the high-level sensorimotor nerve loop involved in the arm motion of human is illustrated in Figure 4. The inputs of the cerebellum include the sensory information from the proprioceptive receptors and the internal

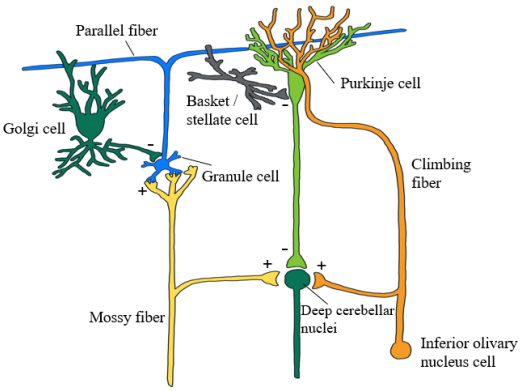

Fig. 3 A simplified schematic representation of the cerebellar structure.

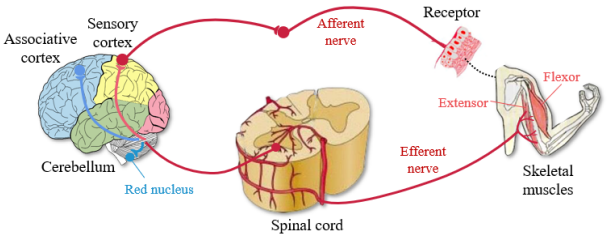

Fig. 4 The sensory and motion signal flow in biological system.

cognitive signals. The outputs are the motor commands transferred to the skeletal muscles via the spinal cord. The major role of the cerebellum is to learn dynamic properties and fine motor control in real-time, and the function of spinal cord is more for information transfer instead of movement control in this work. In the meanwhile, for the skeleton-muscle system, the associative cortex provides a rough internal model of the inverse kinematics [36], and the spinocerebellum-magnocellular red nucleus system acts as a rough inverse dynamic model of the whole system [37]. Generally, in conjunction with these internal models, the cerebellum integrates the actual and desired states to coordinate the muscles and achieve precise elbow motor control.

Inspired by the biological high-level control loop above, Figure 5 illustrates the overall control loop of the artificial arm developed in this work. The aim is to realize the motion control of the elbow joint through the coordinated movements of the two McKibben muscles. During the control process, the reference lengths of the McKibben muscle l_{cal1} and l_{cal2} can be calculated roughly from the desired joint angle θ_d according to the rough inverse kinematics in Equation (1) and Equation (2). Then, with the rough inverse dynamics presented in Equation (3), the pressures applied inside the McKibben muscles can be calculated and reflected in the lengths y_1 and y_2. However, given that the model-uncertainties described as Equation (4) may lead

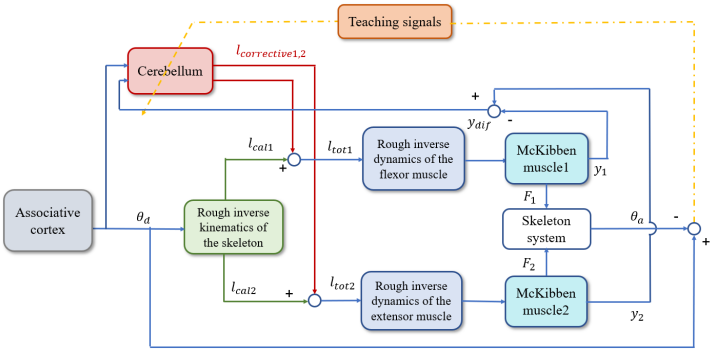

Fig. 5 Schematic of the cerebellar control loop. The control system includes rough inverse models and a cerebellum-like corrective controller. The error information is delivered into the cerebellum-like module to compensate for the deviation of kinematic and dynamic model-uncertainties of the artificial arm.

to the errors between the actual joint angle θ_a and the desired joint angle θ_d during the functioning of the system, a cerebellum-like SNN model is proposed to compensate for the deviation caused by the kinematic and dynamic variations. The target information θ_d and sensory information y_{dif} are encoded as the inputs of the cerebellar model. Furthermore, the error between θ_a and θ_d is taken as a teaching signal to update the cerebellar synapses strength. The cerebellar model plays a pivotal role in acquiring internal models with real-time motor learning. Even though the cerebellum also involves in several other cognitive learning tasks such as classical conditioning and vestibulo-ocular reflex (VOR), it should be noted that the control scheme for the arm movement is different from them in two aspects [17, 38]: (i) The cerebellar model provides corrective reference signals of each muscle to compensate for the model uncertainties and the control loop is organized as a recurrent structure but not a feedforward structure (transferring the reference variables to control variables); (ii) The sensorimotor loop of the arm movement involves spinal cords whereas the eye movement does not.

In this work, the cerebellum control loop is designed as a recurrent architecture. On one hand, this architecture conforms to a range of anatomical and neurophysiological evidence [17] than the cerebellar model in the forward architecture. On the other hand, this architecture has crucial theoretical advantages for adaptive control of nonlinear motor systems, which is proven to be stable when directly using the sensory errors as the cerebellar error signal through Lyapunov analysis [39].

3.2 Cerebellar Network Model

To clarify the working mechanism of the online adaptive learning capability of the cerebellum-like controller, the connectivity and topology of the cerebellar network is depicted in Figure 6, which takes inspiration from the neurobiological studies of mammals as shown in Figure 3. The two afferent of the cerebellar model includes MFs (sensory signals) and IOs (teaching signals), while the efferent is readout through DCNs, corresponding the inputs and outputs in the Figure 5. Briefly, MFs recode the received target and sensory information onto GRs in a sparse state. Then PCs integrate GRs' sensory states through PFs under the supervision of the teaching signal transferred by CFs. Finally, the excitatory signals from MFs as well as the inhibitory signals from PCs are combined in DCNs, which determine the cerebellar outputs and is dedicated to compensating for the reference lengths of the extensor/flexor muscles. For the sake of simplicity, the Basket cells and stellate cells are not included in this model. The synaptic plasticity exists between GRs-PCs and PCs-DCNs. In the cerebellar model, Leaky-integrate-and-fire (LIF) neurons are used to model the dynamic potential properties and temporal spiking activities of realistic neurons [40].

MFs, the major cerebellar afferent interface, encode and transfer both target information and sensory information into the internal cerebellar network. This layer has been equally divided into two groups of 50 fibers. In the first group, each fiber encodes the desired joint angles of the artificial arm θ_d, the another group encodes the length difference between the paired McKibben muscles y_{dif}. The length differences is used as the sensory information instead of the lengths of each muscle to

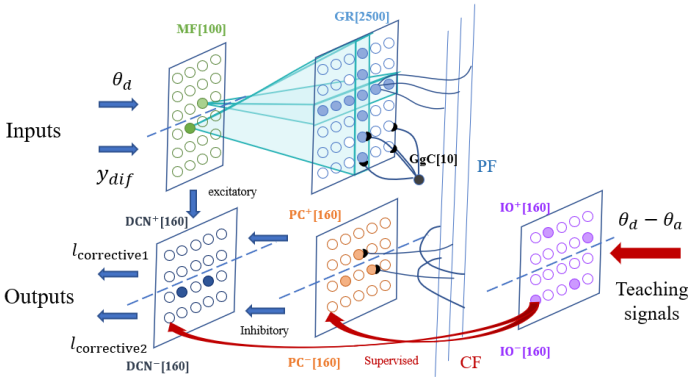

Fig. 6 The structure of the cerebellar model with the schematic representation of the main neural layers, cells and connections. The number after the abbreviation represents the quantity of each kind of fibers or neurons. The teaching signal from CFs modifies the synaptic strength between GR-PCs and PC-DCNs.

reduces the spatial dimensions of the inputs. For the purpose of ensuring the rapid response to time-varying input signals, only a small subset of total MFs are activated to represent current information. This mechanism is closely related to the feature in the cerebellum called "codon representation" [16]. The firing possibilities $P(\delta_{\mathrm{MF_i}}(t))$ is computed by overlapping Radial Basis Functions (RBFs), which is defined as

$$P(\delta_{\mathrm{MF}_i}(t) = 1) = \frac{1}{\sqrt{2\pi}\sigma} \exp\left(-\frac{(x(t) - \mu_i)^2}{2\sigma^2}\right), 0 < i < n_{\mathrm{MF}}, \tag{5}$$

where $x(t)$ is the value of the input variables, μ_i denotes the mathematical expectation and σ denotes the standard deviation of the i^{th} MFs' receptive field, and $\delta_{\mathrm{MF_i}}$ is corresponding to the Dirac delta function of an efferent. For the MFs layer with n neurons, μ_i is uniformly distributed in the sensory range to ensure a small overlap in the response of continuous input.

GRs, the cerebellar layer that holds the most neurons, includes up to 80% of total neurons in human's cerebellum [41]. This layer integrates two inputs conveyed by MFs and generates a sparse representation of current state spaces, which is called the re-coding procedure shown in Figure 7. In fact, the connectivity pattern in MF-GR promotes the non-overlapped neural activation and the distinction of similar input signals. PFs are the output of this layer, carrying the coded sensorimotor information from GRs.

GgCs receive the excitatory inputs from GRs and send inhibitory signals to all GRs. The main function of this layer is preventing large number of GRs from spiking simultaneously, which will lead to ambiguous representations of the state spaces.

IOs convey the teaching signal in the cerebellar network. IOs receive the discrepancy of the desired and actual joint angle from ascending fibers and encode the error signals into spikes. This layer is divided into two subsets named $\mathrm{IO}^+/\mathrm{IO}^-$ to one-to-one connect with PCs and DCNs. Therefore, the errors could affect the synapse

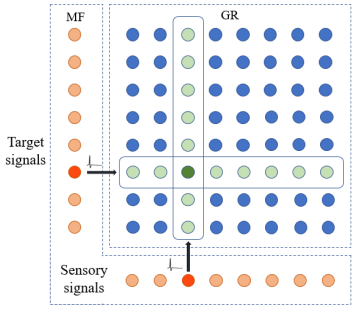

Fig. 7 The topology between MFs and GRs. MFs encoded two kinds of signals (target signal and sensory signals), each MF neuron connects to one row/column of GR neurons. Only when a certain GR neurons is stimulated twice in a time window, the GR neuron will emit a spike.

weight values of PF-PC synapses and PC-DCN synapses with a feedforward structure. Furthermore, the firing rate of each IO neuron is irrelevant to other neurons but only represents corresponding error [42]. Probabilistic Poisson encoding is used to transform the error signals into spiking activities of IOs, which can be denoted as

$$\begin{aligned} \mathrm{P}\left(\sum_{t'=t-T_{\mathrm{iter}}}^{t} \delta_{\mathrm{IO}}(t') = k\right) &= \frac{1}{k!}\varepsilon(t)^{\mathrm{k}} e^{-\varepsilon(t)}, k \in \mathbb{Z}, \\ \varepsilon(t) &= T_{\mathrm{iter}} \min\{\max(K_p \Delta\theta, 1), 10\}, \end{aligned} \tag{6}$$

where δ_{IO} denotes the spiking activities of the IOs, $\sum_{t'=t-T_{\mathrm{iter}}}^{t} \delta_{\mathrm{IO}}(t')$ stands for the total number of spiking emitted in an iteration time T_{iter}, $\varepsilon(t)$ defines the expectation of the firing times in an iteration time, proportional to the joint angle error $\Delta\theta$ and follow the low firing frequency (limited between 1 to 10 Hz) of the electrophysiological results of the real cerebellum [43].

PCs present spiking activities through the online learning mechanism named synaptic plasticity [44]. The divided two subsets $\mathrm{PC}^+/\mathrm{PC}^-$ drive the motion of extensor/flexor muscle respectively. Each PC connects to all PFs to integrate the sparse sensorimotor information propagated from GRs. Simultaneously, it also receives the feedback error signal from corresponding IO neuron to update its synaptic strengths, the detailed learning mechanism will be discussed in Section 3.3.

DCNs are the only output interface of the cerebellar network, whose activity provides the corrective reference lengths of the two McKibben muscles in the control loop. DCNs receive excitatory currents from MFs and IOs and inhibitory currents from PCs, yielding output spiking activities. DCNs are also divided into two subsets $\mathrm{DCN}^+/\mathrm{DCN}^-$, the output of the cerebellar model could be readout from the difference of the spiking activities between the two subsets. The readout function is defined as follows:

$$DCN_{\mathrm{output}}(t) = \int_{t-T_{\mathrm{iter}}}^{t} \sum_{i=1}^{n} \{\delta_{\mathrm{DCN}_{+,i}}(t) - \delta_{\mathrm{DCN}_{-,i}}(t)\} dt, i = 0, 1, .., \frac{1}{2} n_{\mathrm{DCN}} - 1, \tag{7}$$

where δ_{DCN} stands for the spiking activities of DCNs, i defines the neuron index, and $DCN_{\mathrm{output}}(t)$ denotes the outputs of DCNs.

Due to the certain probability in the activities of SNNs over time, it is necessary to smooth the outputs of SNNs, which is similar to human muscles' low-pass filter behaviours [29]. The mean filters used to smooth the outputs are

$$\begin{aligned} L_{\mathrm{corrective}\ 1}(t) &= -\alpha \max\left(\frac{1}{T_f}\int_{t-T_f}^{t} DCN_{\mathrm{output}}(t)dt, 0\right) \\ L_{\mathrm{corrective}\ 2}(t) &= -\beta \max\left(0, -\frac{1}{T_f}\int_{t-T_f}^{t} DCN_{\mathrm{output}}(t)dt\right), \end{aligned} \tag{8}$$

where T_f is the length of kernel, α and β are scale factors from the network outputs to the corrective lengths of McKibben muscles.

3.3 Cerebellar Learning Mechanism

The reason why the cerebellum network could realize adaptive real-time motor learning in our control loop is the learning mechanism occurring at synapses. During repeated exercise in motor learning, the GR-PC and PC-DCN synaptic plasticity are driven by IOs' low-frequency spikes to reduce the motion error. Studies show that cerebellar cells exhibit typical types of synaptic plasticity, more than 15 forms of synaptic plasticity exist in the cerebellar cortex [45]. Long-Term Potentiation (LTP) and Long-Term Depression (LTD) are two typical models of synaptic plasticity for cerebellar learning. The synapses associated with errors will be weakened and other connections will be strengthened [46]. In our work, a Modulated Spike-Timeing-Dependent-Plasticity with Eligibility Trace (MSTDPET) mechanism is adopted to carry out LTP/LTD process to solve the nondeterministic delays [47]. It integrates STDP mechanism with eligibility trace to keep the decay memory of each synapse, standing out in recording temporal dynamic information. Therefore, the cerebellar model could learn to perform accurately under the supervision of feedback error with long delay. Besides, it is also biological plausible to emulate the phenomenon in neural circuit of prefrontal cortex, basal ganglia, and thalamus, in which the eligibility trace plays the role of dopamine [48, 49].

In the learning process, when PCs receive spikes emitted by IOs, the eligibility trace of PFs will be involved in LTD, which ensures the PFs activities in the past period of time could be related to the arriving IO spike. The appearance of LTP is accompanied by the stimulation of PFs and the absence of IOs [50]. The synaptic plasticity balance between LTP and LTD are as follows:

$$\frac{dw_{ij}(t)}{dt} = \frac{LTP_{ij}(t) - LTD_{ij}(t)}{\sum w_{ij}(t)} \tag{9}$$

$$LTP_{ij}(t) = \eta_+ \int \delta_{\mathrm{GR},i}(t) * \overline{\delta_{\mathrm{IO},j}(t)} E_{ij}(t)\, dt \tag{10}$$

$$LTD_{ij}(t) = \eta_- \int \delta_{\mathrm{IO},j}(t) E_{ij}(t)\, dt, \tag{11}$$

where E_{ij} represents the eligibility trace of each synapse, η_+, η_- are the learning rates. The learning rate η is set to the maximum value at the beginning of the learning process and gradually decreases to reach a minimum value as

$$\eta(t) = (\eta_{\max} - \eta_{\min}) e^{-\frac{t}{\tau}} + \eta_{\min}, \tag{12}$$

where τ is the decay constant of the learning rate. In this way, the network not only could approach the desired output in a relatively short time, but also can avoid the problem that the network could not converge. The traces of pre- and postsynaptic activities P_i^+, P_j^- are updated as

$$\begin{aligned} P_i^+(t_0) &= \int_0^{t_0} e^{-\frac{t_0 - t}{\tau_+}} \delta_{\mathrm{GR},i}(t) dt \\ P_j^-(t_0) &= \int_0^{t_0} e^{-\frac{t_0 - t}{\tau_-}} \delta_{\mathrm{PC},j}(t) dt, \end{aligned} \tag{13}$$

where τ_+, τ_- is the decay constant of potential trace. Then the pre- and postsynaptic traces could be convolved with their spiking time and obtain the plasticity dynamics of synapses ζ_{ij} at that time as

$$\zeta_{ij}(t) = P_i^+(t)\delta_{\mathrm{PC},j}(t) + P_j^-(t)\delta_{\mathrm{GR},i}(t). \tag{14}$$

Ultimately, the eligibility trace $E_{ij}(t)$ is updated by integrating with the previous state as

$$E_{ij}(t_0) = \int_0^{t_0} e^{-\left(\frac{t_0 - t}{\tau_1} - \frac{t_0 - t}{\tau_2}\right)} \zeta_{ij}(t) dt, \tag{15}$$

where τ_1, τ_2 ($\tau_1 > \tau_2$) are the decay constant of the eligibility traces.

4 Simulations and Experiments

To evaluate the validity of the proposed cerebellar controller and its synaptic plasticity mechanism, several groups of simulations and experiments are conducted in this section, including precise trajectory following task, anti-perturbation task, and stiffness modulation task. The analyzes of the training performance of the proposed control scheme in terms of training accuracy and stability is then given. Besides, the adaptability and robustness of the proposed cerebellar model is also investigated. These tasks are to demonstrate the promising cerebellar model to control unknown model objects with a extensively adaptable method.

4.1 Simulations

4.1.1 Simulation Setup

In this work, a computer equipped with i7-9700KF CPU and GeForce GTX 1080Ti GPUs is implemented to enable computational efficiency of the SNN-based cerebellar model and control the artificial arm. To realize real-time learning, the iteration time of the network is set as 20 ms. At each iteration, the analog sensory feedback and desired joint angle are encoded to the input spiking activities of network,

Table 1 The neuron model in simulations and experiments.

Neurons type	GRs	GgCs	PCs	DCNs
Neurons number	2500	10	320	320
Refactory period	5 ms	5 ms	1 ms	1 ms
capacitance constant	100 pF	100 pF	100 pF	100 pF
Resting potential	-65 mV	-65 mV	-65 mV	-65 mV
Firing threshold	-58 mV	-52 mV	-42 mV	-52 mV
Potential trace decay constant	-100 mV	-50 mV	-1 mV	-1 mV

Table 2 The synaptic plasticity parameters in simulations and experiments.

Synaptic type	GR-PC	PC-DCN
Synaptic number	800K	51.2K
Synaptic weight range	$[1 \times 10^{-4}$ nS,4 nS]	[0.1 nS,0.08 nS]
Positive learning rate	5×10^{-3}	3×10^{-4}
Negative learning rate	0.3	0.006
Potential trace decay constant	1 ms	1 ms
Eligibility trace decay constant	20 ms, 2.5 ms	20 ms, 2.5 ms
Learning rate decay constant	20000 ms	20000 ms

while the spiking output of the network is decoded into the corrective signals of the skeleton-muscle system and transferred to the low-level controllers. Besides that, the time scale inside the cerebellum-like networks is synchronized with the time inside the simulation platform and real world through system clock. The SNN is established based on PyTorch. The parameter configuration of the SNN in both simulations and experiments is shown in the Table 1, 2. The SNN-based cerebellar model is embedded in Robot Operating System (ROS), and the signal transmission between modules adopts the form of ROS Topics. The simulations of the rough inverse models, as presented in Section 2, are carried out on MATLAB Simulink. The dynamic properties of the simulated McKibben muscle system, including the relationship among internal pressure p_i, the output force F_i and actual length y_i, are modelled through a data-driven system identification method presented in [51]. To realize the best performance, the Mean Square Error (MSE) are computed to evaluate the behaviours and learning efficiency of the cerebellar model over different episodes. It is defined as follows:

$$\mathrm{MSE} = \frac{1}{t_0} \int_{t-t_0}^{t} (\theta_d - \theta_a)^2 dt, \tag{16}$$

where t_0 represents the duration of one episode which equals the cycle of the trajectory.

Since the action execution and sensory information transferring in the brain will cost tens of milliseconds, the time delay is added to the control loop in the simulation to mimic the real biological signal transmission process and communication in real robotic systems. The total delay of transmission and execution of motor commands

is set to be $t_{\text{delay1}} = 50$ ms and the error feedback delay is $t_{\text{delay2}} = 50$ ms. The delay of $t_{\text{delay1}} + t_{\text{delay2}}$ is crucial for the efficiency of traditional controllers, but in the proposed cerebellar model, it is handled by the synaptic plasticity mechanism involving eligibility trace and neuronal potential trace.

4.1.2 Simulation Results

In this subsection, a group of simulations is performed to evaluate the control effect of the proposed cerebellar model which is evolved from multiple episodes and with the absence of any prior knowledge of the controlled object.

At the beginning, the artificial arm requires to follow a low-frequency trajectory with or without the implementation of the cerebellar model. A sine wave with an amplitude of 0.5 rad, a offset of 0.2 rad, and a frequency of 0.2 rad/s is set as the desired joint trajectory. In this task, the velocities of inflation and deflation are relatively slow. In terms of the dynamic properties of McKibben muscles, this slow movement is difficult in maintaining the transient stability. Figure 8 (d) shows the evolution tendency of the control performance with cerebellar model and Figure 8 (g) presents the evaluation criteria of control performance (MSE) of the control scheme. As shown in the figure, the cerebellar model takes about 100 s to converge generally, while the MSE fast decreases to 1.14×10^{-4} rad^2. It also should be noted that the MSEs at different joint positions in the same episode show slightly variation. This is due to the periodicity of the desired trajectory. Nevertheless, the overall trend of the MSEs exhibits a decline over time. Comparing with the controller without the cerebellar model, the proposed controller shows a good capability to compensate for the errors between the desired angle and actual angle caused by model uncertainties. Figure 8 (b) and (c) present the corresponding cerebellar model outputs of DCNs,

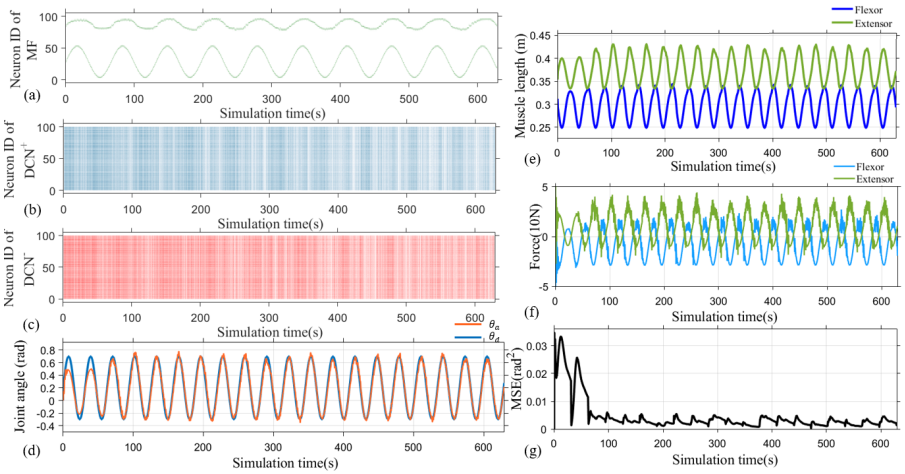

Fig. 8 The overall performance of the proposed control scheme in simulate. The control scheme shows a remarkable capacity to reduce the tracking error with the evolution of synaptic weight.(a)–(c) The spiking activities of MF, DCN$^+$, and DCN$^-$. (d) The desired joint angle and the actual joint angle. (e) The length of extensor and flexor muscles during the learning process. (f) The strain force provided by extensor and flexor muscles. (g) MSE of each learning episode.

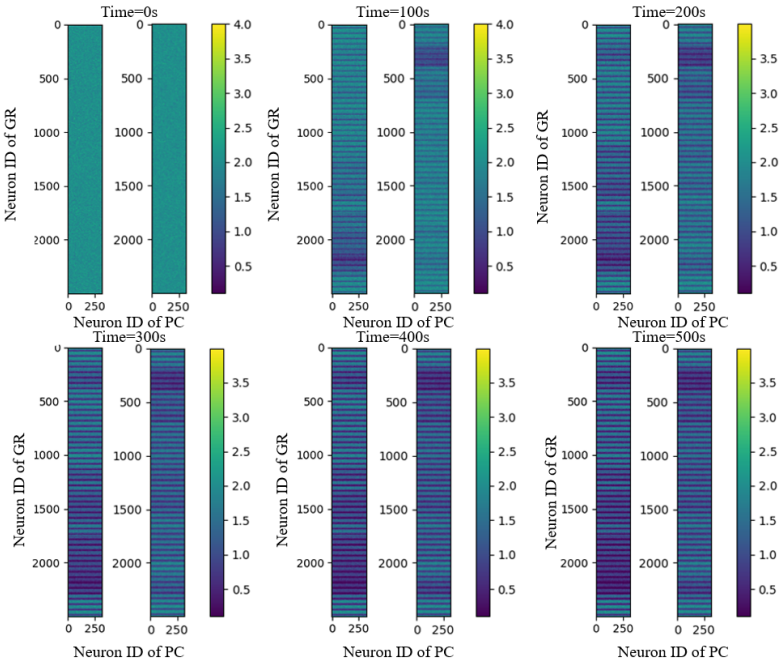

Fig. 9 The synaptic strengths between GRs and PCs after different training time. The thermal diagram at the left side under each time represents the synaptic strengths between GR and PC^{+}, the right side one is the synaptic strengths between GR and PC^{-}.

it indicates that after several circles, the spikes activity of DCNs gradually forms an unique morphology, the distribution of spikes becomes regular and not as dense as before. Figure 8 (e) shows the corrective reference lengths of muscles decoded from DCNs as Equation (8), the length after correction displays better trajectory following accuracy than the calculation results of inverse kinematics. This is caused the system changes caused by the deformation and other dynamical properties. Figure 8 (f) shows the force of two muscles derived from the identification models. The contraction force of flexor muscle and stretch force of extensor muscle forms a antagonistic relationship.

To further analyze the variances inside the cerebellar microcircuits, a closer look are taken at the synaptic connections. Figure 9 records the synaptic strength between GRs and PCs in different moments of the learning process. The synaptic weights are initially set to random values within the range of weight. After 100 s, the striped differences appear in the weights between GRs and PKs. During the motor learning process, the synaptic strengths become lower than the surrounding in some areas. During the last 300 s, these differences become sharper and tend to be steady, which leads to the convergence of the network. The enhanced and weakened synapses are reformed by the control effectiveness.

To verify the ability of the proposed control loop to overcome the environmental inference and variability of the model, some changes are applied in the learning process. At first, external Gaussian noise ε is added to the sensory information and

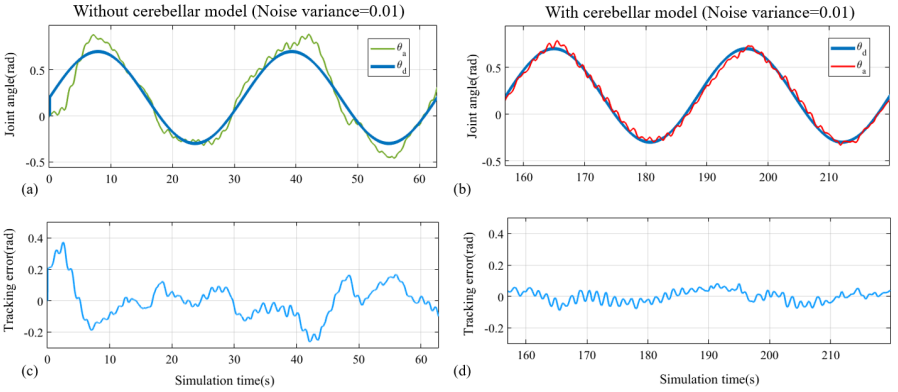

Fig. 10 The control performance when input information is contaminated by Gaussian noise as biological signal processing. The variance of input noise is 0.01. (a) The trajectory following performance without the cerebellar model. (b) Result with the cerebellar model. (c)–(d) The tracking error with/without cerebellar model. More accuracy analysis is shown in Table 3.

Table 3 The MSEs of the whole system when different kind of perturbation are implemented.

Load (g)	Cerebellar model without/with Gaussian Noise						Without cerebellar model
	0	1×10^{-4}	5×10^{-4}	10×10^{-4}	50×10^{-4}	100×10^{-4}	
0	0.00114	0.00162	0.00298	0.00311	0.00392	0.00385	0.00587
50	0.00179	0.00232	0.00208	0.00114	0.00117	0.00740	0.0172
100	0.00658	0.00684	0.00528	0.00541	0.00529	0.00552	0.0383

target information to encoded into MFs. In biological systems, information are represented and transferred by electroneurographic signals, and noises are generated during these procedure and finally received by MFs. Thus, the test results could provides certain understanding of the signal processing in the cerebellum which work against the noises. Figure 10 demonstrates the control performance when Gaussian noise is added to the inputs. Even though the controller without cerebellar model is highly influenced by the propagation of noise integrated with input variables, the cerebellum-inspired corrective controller do not shows distinct instability or accumulation of the noise when it is exposed to perturbed implementation. Further evaluation of control performance when Gaussian noise with different variance are added to the input signals is shown in the Table 3. The cerebellar model successfully improve the robustness of the controller to external noise, which is benefit from the inherent stochasticity of spiking neuronal dynamics. For traditional artificial controller, the fully deterministic use of sensory inputs carries the risk of being susceptible to signal noise and temporal jitter, which leads to the strong overshoot. However, the proposed SNN-based cerebellar model solves this problem by filtering and integrating the discontinuous input spikes in the time window. It is noteworthy that the control performance shows a slight improvement with the presence of faint noise, these slight fluctuations of inputs prevents the network from falling into local optimums.

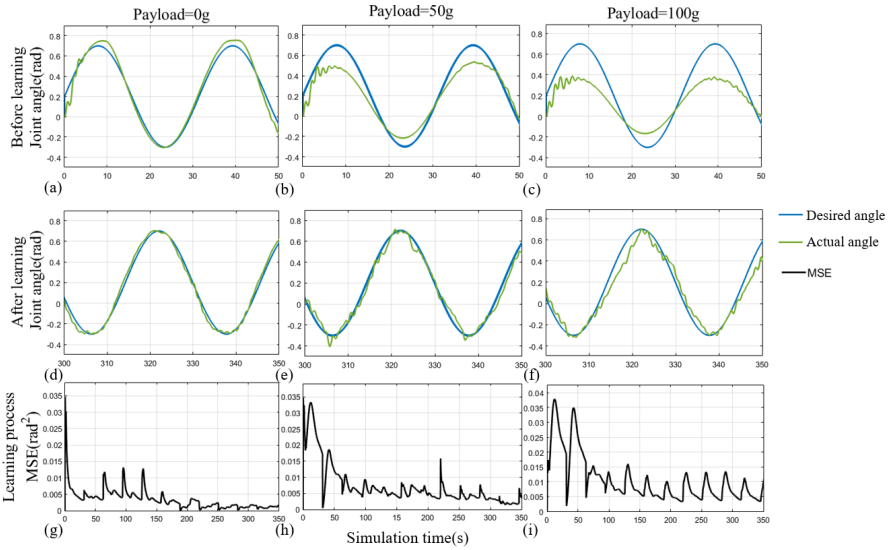

Fig. 11 The desired angle and actual angle of artificial arm when the weight of payloads (0 g, 50 g, 100 g) are attached on the end-effector of the arm in simulations. (a)–(c) At the initial stage (0 to 50 s), the cerebellar model has not obtained the uncertainties of the system, the joint angle is controlled by the rough dynamic model individually. Due to the effect of the gravitational force of the payload, the forces provided by muscles become insufficient and joint angles become smaller simultaneously. (d)–(f) After learning process (300 to 350 s), the cerebellar model adapts to the new dynamics and shows a trajectory following capacities successfully. (g)–(i) MSE of the simulation when 0 g, 50 g, and 100 g payloads are implemented on the artificial arm, the cerebellar model successfully compensates for the system changes.

Secondly, the dynamic model of the whole system is modified by adding an extra payload to the end-effector of the artificial arm. As shown in the Figure 11, the payloads with weight of 50 g and 100 g are mounted on the artificial arm's end-effector, respectively. To point out the effect of cerebellum-like controller, a simulation without cerebellar model is conducted. The system presents evident differences between the desired angle and actual angle with the absence of cerebellum-like controller even through the kinematic properties does not change. The cerebellar model, however, improves the performance roughly within three circle. After about 300 s, the cerebellar model successfully learn to offset the external payload and generate appropriate corrections through motor learning process, which highlights the compensation performance of the cerebellar model. More accuracy evaluation is presented in Table 3.

Under both perturbation, the cerebellum-like SNN successfully adapts to the new properties and presents an outstanding performance without any modification in the network structure and parameters in comparison to the traditional controller. These studies show the adaptability and robustness of the cerebellum-like SNN in the dynamic environment without any prior knowledge. Besides that, the SNN-based controller can potentially enable reverse-engineering the working methodology of the cerebellum on biomimetic soft-body robots.

4.2 Experiments

4.2.1 Experimental Setup

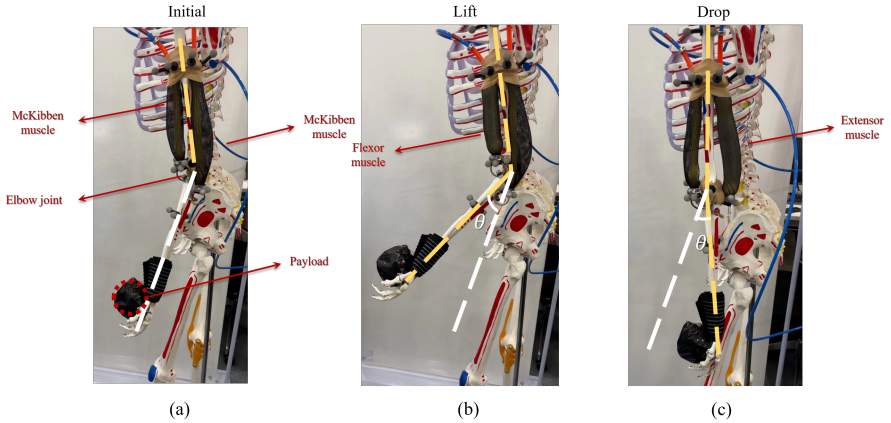

Fig. 12 The experimental platform consisting of a pair of McKibben muscles, the skeleton frame, the payload, and other tubes. (a)–(c) The different states of the artificial arm.

Figure 12 demonstrates the platform used and implemented in the practical experiments. An OptiTrack motion capture system is utilized to measure the sensory information (i.e., the joint angle and muscle lengths information), which consists of six cameras with 1280×1024 resolution and reflective markers fixed on the artificial arm. The real-time coordinates of each marker are recorded to calculate the feedback sensory information. The configuration of the proposed cerebellar model and other modules are similar to the simulations. Besides that, a communication loop is established to realize the information transfer between the controller modules and artificial arm, which is shown in Figure 13. In this loop, the cerebellar model, rough model, and low-level controller are implemented on a computer, while the Optitrack is communicated to the computer via a wireless router. The skeleton-muscle system, microcomputer (Arduino), and computer collaborate through serial communication.

Time delay is an indispensable factor to be considered in real system, which can be caused by GPU processing speed, working frequency of sensors and low-level controller, and the hysteresis of actuators. The time delay of each transmission process in experiments is marked in the figure. The measured 5 to 50 ms delay of the motion capture system outputs is caused by the Ethernet delay of the router, and the 10 ms delay of position feedback is the time delay originally provided by the signal frequency of the Optitrack. The cerebellar model output delay is the required computational time of SNNs determined by hardware computational capacity, which is equal to the iteration time of networks, the 10 ms delay of reference muscle length signal is defined by the fixed step size of Simulation solver, the 40 ms delay of reference pressure signal is caused by the limitation of processing and signal transmission frequency of Arduino, and the switching time of the solenoid-type valves is 10 ms. In

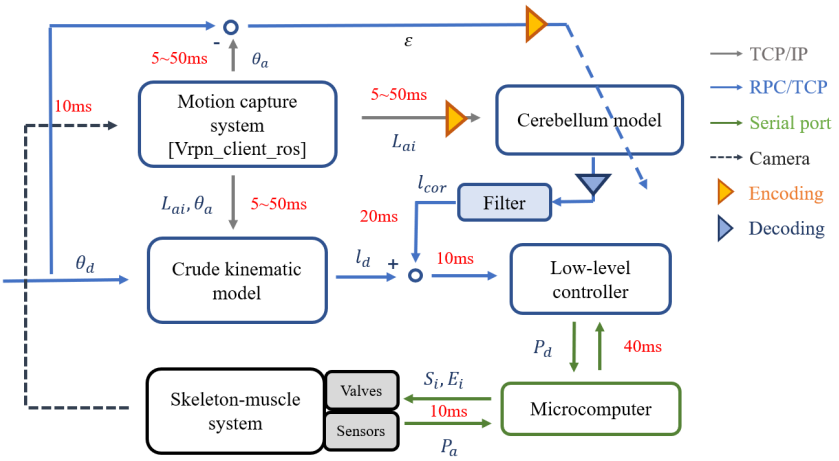

Fig. 13 The signal communication loop between modules.

PC, each signal is labeled by a timestamp, which is synchronized with system time, a ROS Topic named "clock". Such mechanism enables the accumulation of delays and only the signals with the same timestamp could function together.

4.2.2 Experimental Results

For the purpose of providing more profound insight into cerebellar function in motor learning and evaluating the implementation effectiveness of the bionic control method in McKibben muscle control, the control performance of the proposed cerebellar model is tested in a real dynamic environment, a set of experiments are conducted.

In the first group of experiments, the artificial arm is required to follow the sine wave trajectory. This is a kind of repetitive motion of artificial arms which is widely used in rehabilitation equipment [52]. To highlight the online adaptive learning capacity of the proposed cerbellar model, a traditional PID controller tuned by Ziegler-Nichols (Z-N) method is also implemented in the same experiment to replace the function of the cerebellum without any modification in other modules. The results to demonstrate the cerebellar controller's ability to control the artificial arm follow the desired trajectory are shown in Figure 14 (a),(f),(g). To present the learning process, the corrective signal provided by the cerebellar controller is plotted in Figure 14 (e). To qualify the accuracy improvement, the MSEs for each episode are calculated and depicted in Figure 14 (h). As can be seen in the figures, at the initial stage, the actual joint angle is far from following the trajectory due to the uncertainties of the rough model, in the meanwhile, there are frequent oscillations of the trajectory, which destroys the control quality. Moreover, it can be observed that the actual trajectory has a lag compared to the desired trajectory. However, after three episodes, the manipulator gradually tracks the desired trajectory well. In comparison, the arm under PID control exhibits a continuous lag of about 2 s and fails to reach the desired position at the maximum amplitude. In the meanwhile, there are strong jitters in its

motion trajectory, which are caused by the overshoot of the PID controller. Finally, after a period of evolution, the cerebellar model obtained the required coordination ability through the learning procedure. Compared with the original model and PID controller, not only the smoothness of the trajectory peaks is significantly improved, but also the latency is overcome through the learned model.

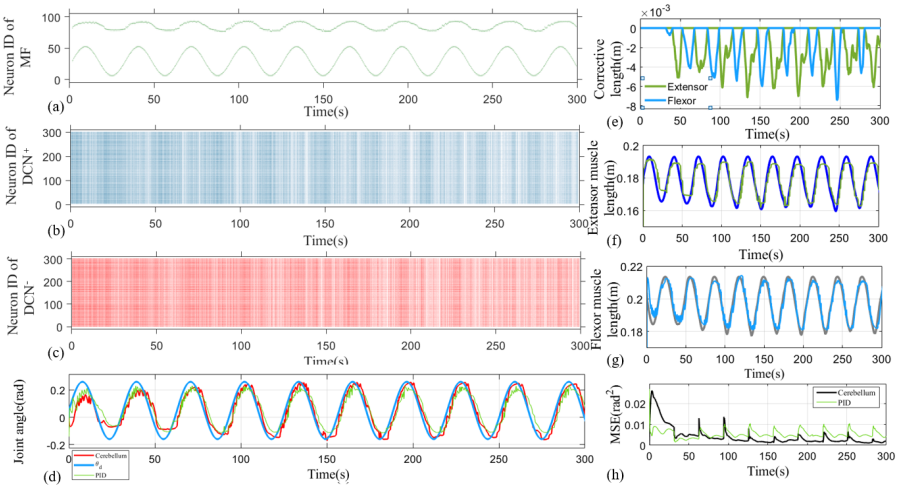

Fig. 14 The control performance of the cerebellar model when completing the trajectory following tasks. (a)–(c) The input and output spiking activities of the SNN. (d) The desired joint angle and actual joint angle of the artificial arm from 0 to 300 s. To verify the capacity of the cerebellar model to compensate for the model uncertainties and delay, the performance of both the PID controller and the cerebellar model are exhibited. (e) The corrective signals provided by the cerebellar model and added to the reference signals of muscle lengths. (f), (g) The comparison of desired and actual lengths of extensor and flexor muscle. (h) The comparison of MSEs between the PID controller and the cerebellar model for each trajectory in one episode.

To test the adaptability and robustness of the proposed cerebellum-like controller to an unstructured and changing environment, further interference experiments are carried out. More specifically, additional weights are added on the end-effector to change the dynamic model of the whole skeleton-muscle system. Here, the cerebellum acts as a compensator to correct the uncertainties that the rough model could not represent. Magnets are used as the payloads to be attached to the end-effector to simulate the behaviours of human's arm lifting the loads. In this scenario, the forces provided by the muscles increase when the manipulator tries to lift the arm to overcome the payloads' gravity and provide a rotational moment for the additional weights.

Figure 15 (a)–(c) demonstrate the learning evolution and control performance of the cerebellar model when payload1 (135 g) and payload2 (90 g) are added at 200 s and removed at 450 s and 575 s, respectively. Figure 15 (d), (e) present the internal changes of muscles. At the moment when the payloads are added, the air pressure of the flexor muscle become higher to provide more force to stabilize the arm, after several learning episodes, the cerebellar controller evolves to provide higher and

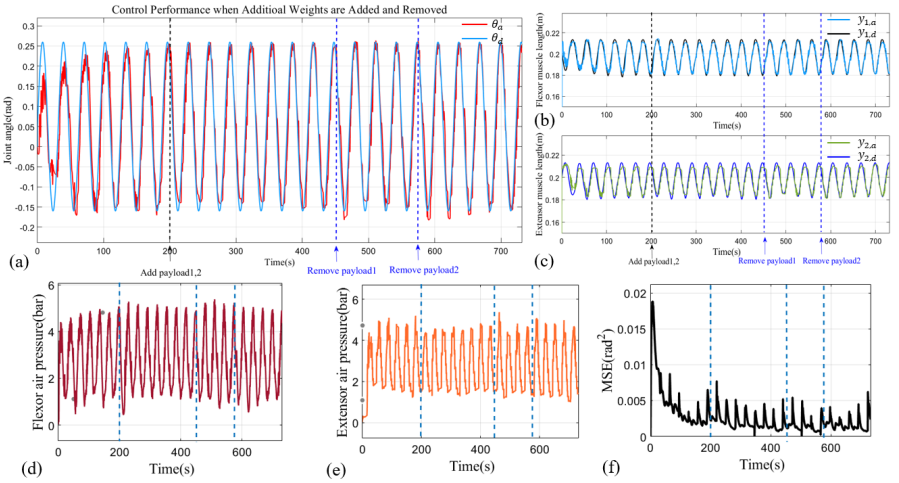

Fig. 15 The controller performance when additional payloads are added (at 200 s) and removed (at 450 s and 575 s) on the end-effector to change the force should be provided by muscles to complete the tasks. (a) The desired joint angle and actual joint angle of the artificial arm from 0 s to 725 s. (b), (c) The comparison of desired and actual lengths of extensor and flexor muscle. (d), (e) The actual air pressure inside the muscles provided by pressure sensors. (f) MSEs of each episodes during the learning procedure.

smoother air pressure to the flexor muscle to compensate for the extra force and precisely follow the desired trajectory again. Similarly, when the payloads are removed, there are surges present in the air pressure of the extensor muscle, which is due to the antagonistic relationship between the two muscles to offset the compensating air pressure provided by flexor muscle before. The cerebellar controller then can adjust its synaptic weights according to the environment uncertainties and changes to achieve the robust control of the artificial arm. It also shows the capability of the cerebellar model to provide extra forces through modifying the desired position.

Finally, the stiffness modulation capacity of the artificial arm is investigated via experiments. Due to the compliance of the McKibben muscles, the artificial arm could adjust the contraction level of the antagonistic muscle pairs to achieve the same position, realizing the stiffness modulation at the joint.

Due to the large torque that the muscle can provide, the effect of the general payload on the muscle cannot be clearly observed, and thus the ability of stiffness modulation cannot be reflected. Therefore, in the experiments, the extensor muscle is stabilized at different constant pressures, providing different muscle stiffness, and the flexor muscles on the other side is controlled by the proposed controller. A Heaviside step function of 0.15 rad is set as the desired joint angle reference. The experimental results with different settings are shown in Figure 16.

Figure 16 (a), (b), and (c) present the step response of the joint angle while the pressure of 2, 3, and 4 Bar is applied inside the extensor muscle, respectively. As can be seen, the proposed controller allows the artificial arm to achieve the desired joint angle after about 50 s. Significantly, low stiffness is with better compliance which allows the system to reach the desired angle without large overshoot and oscillation. In contrast, high stiffness (while the pressure of 4 Bar is applied to the extensor

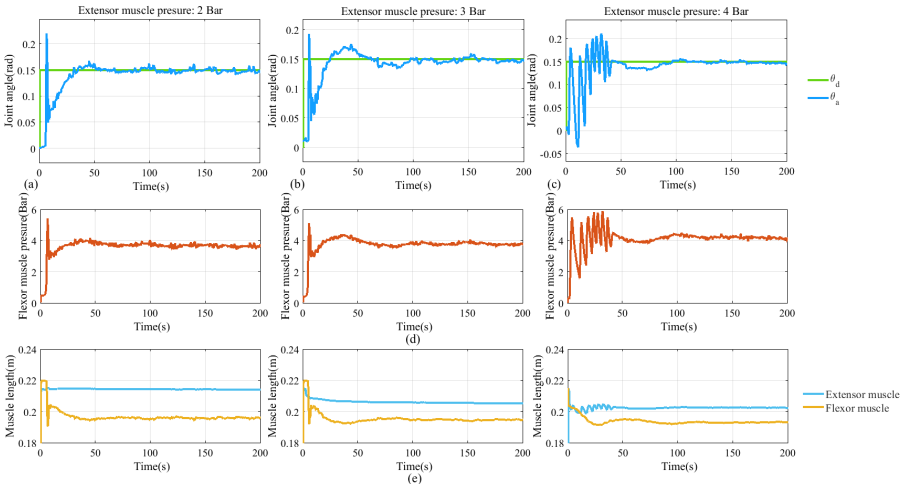

Fig. 16 The stiffness modulation of the artificial arm. An Heaviside step function is applied on the desired joint angle, while the air pressure of the extensor muscle stabilizes at different levels. The results demonstrate the co-contraction capacity of the antagonistic muscle pairs. (a)–(c) The step response of desired joint angle when different constant pressures are applied on extensor muscle. (d) The actual air pressures inside the flexor muscle after desired angle step with different constant pressures applied on extensor muscle. With the increase in muscle contraction on one side, the muscle on the other side also needs to increase the pressure to achieve the same angle. (e) The measured muscle length of the flexor and extensor muscle. The same desired joint angle could be achieve by the co-contraction of muscles on both sides with the increase of stiffness.

muscle) can make the muscle difficult to be deformed, and thus the desired angle cannot be reached smoothly. However, the settling time is not affected significantly and the system is still able to be stabilized at around 100 s. Furthermore, Figure 16 (d) and (e) shows the internal pressure of the flexor muscle and the length changes of both muscles during the step responses with different settings. As can be seen, the internal pressure of the flexor muscle increases as the constant pressure setting of the extensor muscle increases so as to achieve the same desired joint angle. Remarkably, the lengths of both muscles also contract. It indicates that the proposed method allows the developed arm in antagonistic pairs for co-contraction capability which is crucial for adapting to tasks with different loads or impedance.

4.3 Discussion

From both simulation and experimental results, it can be found that the proposed system can track the desired joint angular trajectories accurately with different payload configurations. Additionally, by comparing results between the proposed controller and PID controller, it is obvious that the proposed controller outperforms the PID controller. In summary, the proposed controller facilitates the developed antagonistic McKibben muscles to achieve good trajectory tracking performance as well as strong robustness. Furthermore, the co-contraction capacity of the antagonistic muscle pairs has been evaluated while results show that the proposed method allows for stiffness modulation which is vital in human-robot interaction.

5 Conclusion

In this paper, the control challenges of an antagonistic pair of McKibben muscles are investigated, which lie in the model uncertainties in the coupled dynamic and kinematic model of the skeleton-muscle system and communication delays. To this end, a McKibben muscle-actuated artificial arm inspired by human elbows is developed. Moreover, a cerebellum-inspired SNN is proposed to compensate for the model uncertainties and overcome the signal delay. In addition, the corresponding control scheme and system communication architecture are designed.

Finally, both simulations and experiments are conducted to validate the effectiveness and performance of the proposed cerebellum-like controller and the soft artificial arm system. The results show that the McKibben muscle-actuated soft arm can track the desired trajectory well and precisely under the proposed control scheme, even when the dynamic model is changed. The modulation of the joint stiffness is also available. This is due to the good adaptability of the cerebellar model. Therefore, it can be concluded that the proposed bio-inspired control approach of antagonistic McKibben muscles can achieve good trajectory tracking performance and strong robustness to model uncertainties and disturbances. However, this paper mainly investigates the controller for one antagonistic muscle pairs (1-DoF joint) and the closed-loop frequency is limited by the hardware. Therefore, the future works include the controller design for multi-DoF artificial arm and processing frequency enhancement for the control system.

Acknowledgements This work was supported by the National Natural Science Foundation, China (No.62173300).

Data availability The datasets and source code that support the current study are available from the corresponding author on reasonable request.

Declarations

Conflict of interest The authors have no conflicts of interest to declare.

References

[1] Robinson R.M., Kothera C.S., Sanner R.M., Wereley N.M. (2016). Nonlinear control of robotic manipulators driven by pneumatic artificial muscles. *IEEE/ASME Transactions on Mechatronics*, *21*(1), 55–68. https://doi.org/10.1109/TMECH.2015.2483520

[2] Jahanabadi H., Mailah M., Zain M.Z.M., Hooi H.M. (2011). Active force with fuzzy logic control of a two-link arm driven by pneumatic artificial muscles. *Journal of Bionic Engineering*, *8*(4), 474–484. https://doi.org/10.1016/S1672-6529(11)60053-X

[3] Huang J., Tu X.K., He J.P. (2016). Design and evaluation of the RUPERT wearable upper extremity exoskeleton robot for clinical and in-home therapies. *IEEE Transactions on Systems, Man, and Cybernetics: Systems*, *46*(7), 926–935. https://doi.org/10.1109/TSMC.2015.2497205

[4] Bicchi A., Tonietti G. (2004). Fast and "soft-arm" tactics [robot arm design]. *IEEE Robotics Automation Magazine*, *11*(2), 22–33. https://doi.org/10.1109/MRA.2004.1310939

[5] Song Y.S., Sun Y., Brand van den R., Zitzewitz von J., Micera S., Courtine G., Paik J. (2013). Soft robot for gait rehabilitation of spinalized rodents. in *2013 IEEE/RSJ International Conference on Intelligent Robots and Systems*, pp. 971–976. https://doi.org/10.1109/IROS.2013.6696468

[6] Tondu B., Ippolito S., Guiochet J., Daidie A. (2005). A seven-degrees-of-freedom robot-arm driven by pneumatic artificial muscles for humanoid robots. *The International Journal of Robotics Research*, *24*(4), 257–274. https://doi.org/10.1177/0278364905052437

[7] Meller M., Kogan B., Bryant M., Garcia E. (2018). Model-based feedforward and cascade control of hydraulic mckibben muscles. *Sensors and Actuators A: Physical*, *275*, 88–98. https://doi.org/10.1016/j.sna.2018.03.036

[8] Minh T.V., Tjahjowidodo T., Ramon H., Van Brussel H. (2009). Control of a pneumatic artificial muscle (pam) with model-based hysteresis compensation. in *2009 IEEE/ASME International Conference on Advanced Intelligent Mechatronics*, pp. 1082–1087. https://doi.org/10.1109/AIM.2009.5229730

[9] Andrikopoulos G., Nikolakopoulos G., Manesis S. (2014). Advanced nonlinear pid-based antagonistic control for pneumatic muscle actuators. *IEEE Transactions on Industrial Electronics*, *61*(12), 6926–6937. https://doi.org/10.1109/TIE.2014.2316255

[10] Lilly J. (2003). Adaptive tracking for pneumatic muscle actuators in bicep and tricep configurations. *IEEE Transactions on Neural Systems and Rehabilitation Engineering*, *11*(3), 333–339. https://doi.org/10.1109/TNSRE.2003.816870

[11] Caldwell D., Medrano-Cerda G., Goodwin M. (1994). Characteristics and adaptive control of pneumatic muscle actuators for a robotic elbow. in *Proceedings of the 1994 IEEE International Conference on Robotics and Automation*, vol. 4, pp. 3558–3563. https://doi.org/10.1109/ROBOT.1994.351573

[12] Hesselroth T., Sarkar K., Smagt van der P., Schulten K. (1994). Neural network control of a pneumatic robot arm. *IEEE Transactions on Systems, Man, and Cybernetics*, *24*(1), 28–38. https://doi.org/10.1109/21.259683

[13] Ai Q.S., Ke D., Zuo J., Meng W., Liu Q., Zhang Z.Q., Xie S.Q. (2020). High-order model-free adaptive iterative learning control of pneumatic artificial muscle with enhanced convergence. *IEEE Transactions on Industrial Electronics*, *67*(11), 9548–9559. https://doi.org/10.1109/TIE.2019.2952810

[14] Ahn K.K., Anh H.P.H. (2009). Design and implementation of an adaptive recurrent neural networks (ARNN) controller of the pneumatic artificial muscle (PAM) manipulator. *Mechatronics*, *19*(6), 816–828. https://doi.org/10.1016/J.MECHATRONICS.2009.04.006

[15] Albus J.S. (1971). A theory of cerebellar function. *Mathematical Biosciences*, *10*(1-2), 25–61. https://doi.org/https://doi.org/10.1016/0025-5564(71)90051-4

[16] Marr D., Thach W.T. (1969). A theory of cerebellar cortex. *Journal of Physiology*, *202*, 437. https://doi.org/https://doi.org/10.1007/978-1-4684-6775-8_3

[17] Porrill J., Dean P., Anderson S.R. (2013). Adaptive filters and internal models: multilevel description of cerebellar function. *Neural Networks*, *47*, 134–149. https://doi.org/10.1016/j.neunet.2012.12.005

[18] Lenz A., Anderson S.R., Pipe A.G., Melhuish C., Dean P., Porrill J. (2009). Cerebellar-inspired adaptive control of a robot eye actuated by pneumatic artificial muscles. *IEEE Transactions on Systems, Man, and Cybernetics, Part B (Cybernetics)*, *39*(6), 1420–1433. https://doi.org/10.1109/TSMCB.2009.2018138

[19] Zhao W., Song A.G. (2020). Active motion control of a knee exoskeleton driven by antagonistic pneumatic muscle actuators. *Actuators*, *9*(4), 134. https://doi.org/10.3390/act9040134

[20] Chi H.Z., Su H.R., Liang W.Y., Ren Q.Y. (2021). Control of a rehabilitation robotic device driven by antagonistic soft actuators. *Actuators*, *10*(6). https://doi.org/10.3390/act10060123

[21] Ohta P., Valle L., King J., Low K., Yi J., Atkeson C.G., Park Y.L. (2018). Design of a lightweight soft robotic arm using pneumatic artificial muscles and inflatable sleeves. *Soft robotics*, *5*(2), 204–215. https://doi.org/10.1089/soro.2017.0044

[22] Andrikopoulos G., Nikolakopoulos G. (2018). Humanoid robotic leg via pneumatic muscle actuators: Implementation and control. *Meccanica*, *53*(1), 465–480. https://doi.org/10.1007/s11012-017-0738-6

[23] Wolfen S., Walter J., Günther M., Häufle D., Schmitt S. (2018). Bioinspired pneumatic muscle spring units mimicking the human motion apparatus: benefits for passive motion range and joint stiffness variation in antagonistic setups. in *2018 25th International Conference on Mechatronics and Machine Vision in*

Practice (M2VIP), pp. 1–6. https://doi.org/10.1109/M2VIP.2018.8600913

[24] Driess D., Schmitt S., Toussaint M. (2019). Active Inverse Model Learning with Error and Reachable Set Estimates. in *2019 IEEE/RSJ International Conference on Intelligent Robots and Systems (IROS)*, pp. 1826–1833. https://doi.org/10.1109/IROS40897.2019.8967858

[25] Driess D., Zimmermann H., Wolfen S., Suissa D., Haeufle D., Hennes D., Toussaint M., Schmitt S. (2018). Learning to control redundant musculoskeletal systems with neural networks and SQP: exploiting muscle properties. in *2018 IEEE International Conference on Robotics and Automation (ICRA)*, pp. 6461–6468. https://doi.org/10.1109/ICRA.2018.8463160

[26] Hodgkin A.L., Huxley A.F. (1952). A quantitative description of membrane current and its application to conduction and excitation in nerve. *The Journal of physiology*, *117*(4), 500. https://doi.org/10.1113/jphysiol.1952.sp004764

[27] Albus J.S. (1975). A new approach to manipulator control: The cerebellar model articulation controller (CMAC). *Journal of Dynamic Systems, Measurement, and Control*, *97*, 220–227. https://doi.org/10.1115/1.3426922

[28] Pfeiffer M., Pfeil T. (2018). Deep learning with spiking neurons: Opportunities and challenges. *Frontiers in Neuroscience*, *12*, 774. https://doi.org/10.3389/fnins.2018.00774

[29] Abadia I., Naveros F., Ros E., Carrillo R., Luque N. (2021). A cerebellar-based solution to the nondeterministic time delay problem in robotic control. *Science Robotics*, *6*(58), eabf2756. https://doi.org/10.1126/scirobotics.abf2756

[30] Stromatias E., Neil D., Pfeiffer M., Galluppi F., Furber S., Liu S.C. (2015). Robustness of spiking Deep Belief Networks to noise and reduced bit precision of neuro-inspired hardware platforms. *Frontiers in Neuroscience*, *9*. https://doi.org/10.3389/fnins.2015.00222

[31] Chao E.Y., Morrey B.F. (1978). Three-Dimensional rotation of the elbow. *Journal of Biomechanics*, *11*(1-2), 57,73–71,73. https://doi.org/10.1016/0021-9290(78)90044-1

[32] Vannucci L., Falotico E., Laschi C. (2017). Proprioceptive feedback through a neuromorphic muscle spindle model. *Frontiers in Neuroscience*, *11*, 341. https://doi.org/10.3389/fnins.2017.00341

[33] Chou C.P., Hannaford B. (1996). Measurement and modeling of McKibben pneumatic artificial muscles. *IEEE Transactions on Robotics and Automation*, *12*(1), 90–102. https://doi.org/10.1109/70.481753

[34] Tondu B. (2012). Modelling of the McKibben artificial muscle: A review. *Journal of Intelligent Material Systems and Structures*, *23*(3), 225–253. https://doi.org/10.1177/1045389X11435435

[35] Eccles J., Ito M., Szentágothai J. (1967). *The cerebellum as a neuronal machine*. Springer Berlin Heidelberg. https://doi.org/10.1007/978-3-662-13147-3

[36] Siciliano B., Khatib O. (2008). *Springer handbook of robotics*. Springer Berlin Heidelberg. https://doi.org/10.1007/978-3-540-30301-5_58

[37] Kawato K., M. Furukawa, Suzuki R. (1987). A hierarchical neural-network model for control and learning of voluntary movement. *Biological Cybernetics*, *57*(3), 169–185. https://doi.org/10.1007/BF00364149

[38] Kawato M. (1999). Internal models for motor control and trajectory planning. *Current Opinion in Neurobiology*, *9*(6), 718–727. https://doi.org/10.1016/S0959-4388(99)00028-8

[39] Porrill J., Dean P. (2007). Recurrent cerebellar loops simplify adaptive control of redundant and nonlinear motor systems. *Neural Computation*, *19*(1), 170–193. https://doi.org/10.1162/neco.2007.19.1.170

[40] Gerstner W., Kistler M. W. (2002). *Spiking neuron models: Single neurons, populations, plasticity*. Cambridge University Press. https://doi.org/10.1017/CBO9780511815706

[41] Herculano-Houzel (2010). Coordinated scaling of cortical and cerebellar numbers of neurons. *Frontiers in Neuroanatomy*, *4*, 12. https://doi.org/10.3389/fnana.2010.00012

[42] Walberg F. (1956). Descending connections to the inferior olive. an experimental study in the cat. *Journal of Comparative Neurology*, *104*(1), 77–173. https://doi.org/https://doi.org/10.1002/cne.901040107

[43] Ohtsuki G., Piochon C., Hansel C. (2009). Climbing fiber signaling and cerebellar gain control. *Frontiers in Cellular Neuroscience*, *3*, 4. https://doi.org/10.3389/neuro.03.004.2009

[44] Medina J., Lisberger S. (2008). Corrigendum: Links from complex spikes to local plasticity and motor learning in the cerebellum of awake-behaving monkeys. *Nature neuroscience*, *11*(10), 1185–92. https://doi.org/10.1038/nn.2197

[45] D'Angelo E., Mapelli L., Casellato C., Garrido J., Luque N., Monaco J., Prestori F., Pedrocchi A., Ros E. (2015). Distributed circuit plasticity: New clues for the cerebellar mechanisms of learning. *Cerebellum*, *15*(2), 139–151. https://doi.org/10.1007/s12311-015-0711-7

[46] Ito M. (2001). Cerebellar long-term depression: Characterization, signal transduction, and functional roles. *Physiological Reviews*, *81*(3), 1143–95. https://doi.org/10.1152/physrev.2001.81.3.1143

[47] Florian R.V. (2007). Reinforcement learning through modulation of spike-timing-dependent synaptic plasticity. *Neural Computation*, *19*(6), 1468–1502. https://doi.org/10.1162/neco.2007.19.6.1468

[48] Seamans J.K., Yang C.R. (2004). The principal features and mechanisms of dopamine modulation in the prefrontal cortex. *Progress in Neurobiology*, *74*(1), 321–321. https://doi.org/doi.org/10.1016/j.pneurobio.2004.10.002

[49] Huang Y.Y., Simpson E., Kellendonk C., Kandel E.R. (2004). Genetic evidence for the bidirectional modulation of synaptic plasticity in the prefrontal cortex by d1 receptors. *Proceedings of the National Academy of Sciences*, *101*(9), 3236–3241. https://doi.org/https://doi.org/10.1073/pnas.0308280101

[50] Hirano T. (1990). Depression and potentiation of the synaptic transmission between a granule cell and a purkinje cell in rat cerebellar culture. *Neuroscience Letters*, *119*(2), 141–144. https://doi.org/https://doi.org/10.1016/0304-3940(90)90818-T

[51] Liang W.Y., Cao J.W., Ren Q.Y., Xu J.X. (2019). Control of dielectric elastomer soft actuators using antagonistic pairs. *IEEE/ASME Transactions on Mechatronics*, *24*(6), 2862–2872. https://doi.org/10.1109/TMECH.2019.2945518

[52] Xing K.X., Huang J., Xu Q., Wang Y.J. (2009). Design of a wearable rehabilitation robotic hand actuated by pneumatic artificial muscles. in *2009 7th Asian Control Conference*, pp. 740–744